Published for SISSA by Springer

Received: May 10, 2018
Accepted: June 7, 2018
Published: June 18, 2018

Measurement of CP violation in $B^0 \to D^{\mp}\pi^{\pm}$ decays

The LHCb collaboration

E-mail: alex.birnkraut@tu-dortmund.de

Abstract: A measurement of the CP asymmetries S_f and $S_{\bar{f}}$ in $B^0 \to D^{\mp}\pi^{\pm}$ decays is reported. The decays are reconstructed in a dataset collected with the LHCb experiment in proton-proton collisions at centre-of-mass energies of 7 and 8 TeV and corresponding to an integrated luminosity of $3.0\,\text{fb}^{-1}$. The CP asymmetries are measured to be $S_f = 0.058 \pm 0.020(\text{stat}) \pm 0.011(\text{syst})$ and $S_{\bar{f}} = 0.038 \pm 0.020(\text{stat}) \pm 0.007(\text{syst})$. These results are in agreement with, and more precise than, previous determinations. They are used to constrain angles of the unitarity triangle, $|\sin(2\beta+\gamma)|$ and γ, to intervals that are consistent with the current world-average values.

Keywords: B physics, CKM angle gamma, CP violation, Flavor physics, Hadron-Hadron scattering (experiments)

ArXiv ePrint: 1805.03448

https://doi.org/10.1007/JHEP06(2018)084

JHEP06(2018)084

Contents

JHEP06(2018)084

1 Introduction

In the Standard Model, the decays $B^0 \to D^-\pi^+$ and $B^0 \to D^+\pi^-$ proceed through the $\bar{b} \to \bar{c}u\bar{d}$ and $\bar{b} \to \bar{u}c\bar{d}$ quark transitions, respectively.[1] The relative weak phase between these two decay amplitudes is $\gamma \equiv \arg(-V_{ud}V_{ub}^*/V_{cd}V_{cb}^*)$. The B^0 meson can undergo a flavour oscillation before the decay. The amplitude of the direct decay and that of a decay preceded by an oscillation have a total relative phase difference of $2\beta + \gamma$, where $\beta \equiv \arg(-V_{cd}V_{cb}^*/V_{td}V_{tb}^*)$. The phases β and γ are angles of the unitary triangle. Measurements of *CP* violation in $B^0 \to D^\mp\pi^\pm$ decays provide information on these angles.

Decay-time-dependent *CP* asymmetries in $B^0 \to D^\mp\pi^\pm$ decays can be measured by analysing the decay rates as a function of the decay time of B^0 mesons of known initial flavour [1–3]. The ratio of the decay amplitudes, $r_{D\pi} = |A(B^0 \to D^+\pi^-)/A(B^0 \to D^-\pi^+)|$, is around 2%, and limits the size of the *CP* asymmetries. Given its small value, this ratio needs to be determined from independent measurements, for example using the branching ratio of $B^0 \to D_s^+\pi^-$ decays under the assumption of SU(3) flavour symmetry [4, 5].

The decay rates of initially produced B^0 mesons to the final states $f = D^-\pi^+$ and $\bar{f} = D^+\pi^-$ as a function of the B^0-meson decay time, t, are given by

$$\begin{aligned} \Gamma_{B^0\to f}(t) &\propto e^{-\Gamma t}\left[1 + C_f\cos(\Delta m\, t) - S_f\sin(\Delta m\, t)\right], \\ \Gamma_{B^0\to \bar{f}}(t) &\propto e^{-\Gamma t}\left[1 + C_{\bar{f}}\cos(\Delta m\, t) - S_{\bar{f}}\sin(\Delta m\, t)\right], \end{aligned} \tag{1.1}$$

[1] Inclusion of charge conjugate modes is implied unless explicitly stated.

where Γ is the average B^0 decay width and Δm is the B^0–$\overline{B}^0$ oscillation frequency. For an initially produced $\overline{B}^0$ meson, the same equations hold except for a change of sign of the coefficients in front of the sine and cosine functions. No *CP* violation in the decay is assumed, i.e. only tree-level processes contribute to the decay amplitudes. It is also assumed that $|q/p| = 1$, where q and p are the complex coefficients defining the heavy and light mass eigenstates of the B^0 system, and $\Delta\Gamma = 0$, where $\Delta\Gamma$ is the decay-width difference between the two mass eigenstates. These assumptions follow from the known values of these quantities [6]. Under these assumptions, the coefficients of the cosine and sine terms of eq. (1.1) are given by

$$C_f = \frac{1 - r_{D\pi}^2}{1 + r_{D\pi}^2} = -C_{\bar{f}}\,, \tag{1.2}$$

$$S_f = -\frac{2r_{D\pi}\sin\left[\delta - (2\beta + \gamma)\right]}{1 + r_{D\pi}^2}\,, \tag{1.3}$$

$$S_{\bar{f}} = \frac{2r_{D\pi}\sin\left[\delta + (2\beta + \gamma)\right]}{1 + r_{D\pi}^2}\,, \tag{1.4}$$

where δ is the *CP*-conserving phase difference between the $\bar{b} \to \bar{c}u\bar{d}$ and $\bar{b} \to \bar{u}c\bar{d}$ decay amplitudes. Due to the small value of $r_{D\pi}$, terms of $\mathcal{O}(r_{D\pi}^2)$ are neglected in this analysis, fixing $C_f = -C_{\bar{f}} = 1$.

A measurement of the *CP* asymmetries S_f and $S_{\bar{f}}$ can be interpreted in terms of $2\beta+\gamma$ by using the value of $r_{D\pi}$ as input. Additionally, using the known value of β [6], the angle γ can be evaluated. The determination of γ from tree-level decays is important because processes beyond the Standard Model are not expected to contribute. Constraints from the analysis of $B^0 \to D^{\mp}\pi^{\pm}$ decays can be combined with other measurements to improve the ultimate sensitivity to this angle [7].

Measurements of S_f and $S_{\bar{f}}$ using $B^0 \to D^{(*)\mp}\pi^{\pm}$ and $B^0 \to D^{\mp}\rho^{\pm}$ decays have been reported by the BaBar [8, 9] and Belle [10, 11] collaborations. This paper presents a measurement of S_f and $S_{\bar{f}}$ with $B^0 \to D^{\mp}\pi^{\pm}$ decays reconstructed in a dataset collected with the LHCb experiment in proton-proton collisions at centre-of-mass energies of 7 and 8 TeV and corresponding to an integrated luminosity of $3.0\,\text{fb}^{-1}$. This is the first measurement of S_f and $S_{\bar{f}}$ at a hadron collider.

2 Detector and simulation

The LHCb detector [12, 13] is a single-arm forward spectrometer covering the pseudorapidity range 2–5, designed for the study of particles containing b or c quarks. The detector includes a high-precision tracking system consisting of a silicon-strip vertex detector surrounding the pp interaction region [14], a large-area silicon-strip detector located upstream of a dipole magnet with a bending power of about 4 Tm, and three stations of silicon-strip detectors and straw drift tubes [15] placed downstream of the magnet. The tracking system provides a measurement of the momentum, p, of charged particles with a relative uncertainty that varies from 0.5% at low momentum to 1.0% at 200 GeV/c. The minimum distance of a track to a primary vertex (PV), the impact parameter (IP), is measured with a resolution of $(15 + 29/p_{\text{T}})\,\mu\text{m}$, where p_{T} is the component of the momentum

JHEP06(2018)084

transverse to the beam, in GeV/c. Different types of charged hadrons are distinguished using information from two ring-imaging Cherenkov detectors. Photons, electrons and hadrons are identified by a calorimeter system consisting of scintillating-pad and preshower detectors, an electromagnetic calorimeter and a hadronic calorimeter. Muons are identified by a system composed of alternating layers of iron and multiwire proportional chambers.

In the simulation, pp collisions are generated using Pythia [16, 17] with a specific LHCb configuration [18]. Decays of hadronic particles are described by EvtGen [19], in which final-state radiation is generated using Photos [20]. The interaction of the generated particles with the detector, and its response, are implemented using the Geant4 toolkit [21, 22] as described in ref. [23].

3 Candidate selection

The online event selection is performed by a trigger, which consists of a hardware stage, using information from the calorimeter and muon systems, followed by a software stage, which applies a full event reconstruction. Events containing a muon with high p_{T} or a hadron, photon or electron with high transverse energy in the calorimeters are considered at the hardware trigger stage. Events selected by the trigger using hadrons from the signal decay represent 70% of the sample used in this analysis, the rest being collected using trigger criteria satisfied by other properties of the event.

The software trigger requires a two-, three-, or four-track secondary vertex with a significant displacement from the primary pp interaction vertices. At least one charged particle must have $p_{\mathrm{T}} > 1.7\,\mathrm{GeV}/c$ and be inconsistent with originating from a PV. A multivariate algorithm is used for the identification of secondary vertices consistent with the decay of a b hadron [24].

The selection of $B^0 \to D^{\mp}\pi^{\pm}$ candidates is performed by reconstructing $D^- \to K^+\pi^-\pi^-$ candidates from charged particle tracks with high momentum and transverse momentum, and originating from a common displaced vertex. Particle identification (PID) information is used to select kaon and pion candidates, and the $K^+\pi^-\pi^-$ invariant mass is required to be within $35\,\mathrm{MeV}/c^2$ of the known value of the D^- mass [25]. These candidates are combined with a fourth charged particle, referred to as the *companion*, to form the B^0 vertex, which must be displaced from any PV. The PV with respect to which the B^0 candidate has the smallest χ^2_{IP} is considered as the production vertex. The χ^2_{IP} is defined as the difference in the vertex-fit χ^2 of a given PV reconstructed with and without the B^0 candidate. No PID requirement is applied to the companion track at this stage.

The $B^0 \to D^{\mp}\pi^{\pm}$ candidates are required to match the secondary vertices found in the software trigger, to have a proper decay time larger than 0.2 ps, and to have a momentum vector aligned with the vector formed by joining the PV and the B^0 decay vertex. The decay time is determined from a kinematic fit in which the B^0 candidate is constrained to originate from the PV to improve the decay-time resolution, while the B^0-candidate mass is computed assigning the known value [25] to the mass of the D^- candidate to improve the mass resolution [26]. A combination of PID information and mass-range vetoes is used to

JHEP06(2018)084

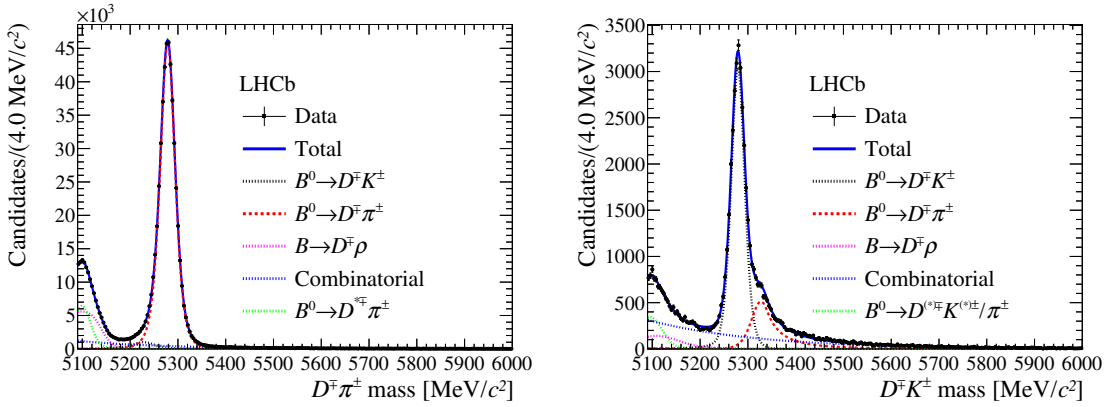

Figure 1. Invariant mass distributions of the (left) pion-like and (right) kaon-like samples with fit projections overlaid. The simultaneous fit of the two distributions is described in the text and yields a χ^2 per degree of freedom of 1.18. The $B \to D^\mp \rho$ component includes both $B^0 \to D^\mp \rho^\pm$ and $B^\mp \to D^\mp \rho^0$ decays.

suppress to a negligible level cross-feed backgrounds such as $\Lambda_b^0 \to \Lambda_c^+ (\to pK^-\pi^+)\pi^-$ and $B_s^0 \to D_s^- (\to K^-K^+\pi^-)\pi^+$, due to the misidentification of protons and kaons as pions.

A boosted decision tree (BDT) [27, 28] is used to increase the signal purity by suppressing background from random combinations of particles. Candidates reconstructed from simulated $B^0 \to D^\mp \pi^\pm$ decays are used as signal in the training of the BDT, and data candidates with an invariant mass larger than 5.5 GeV/c^2 are used as background. A set of 16 variables are combined into a single response, which is used to categorise the B^0 candidates. The most relevant variables entering the BDT are the quality of the fit of the B^0 vertex and that of the kinematic fit to calculate the B^0 decay time, the transverse momentum of the D^- candidate, and the quality of the fit of the companion-particle track. The requirement placed on the BDT response is chosen to maximise the expected sensitivity to S_f and $S_{\bar{f}}$ as derived from a set of simulated samples of signal plus background that are passed through the entire analysis. The data sample is further required to consist of B^0 candidates whose initial flavour has been determined by means of the flavour tagging algorithms described in section 5.

4 Sample composition

The data sample after the selection is split into two disjoint subsets according to the PID information of the companion particle: a sample referred to as *pion-like* consisting mostly of genuine $B^0 \to D^\mp \pi^\pm$ decays, and a sample referred to as *kaon-like* consisting mostly of genuine $B^0 \to D^\mp K^\pm$ decays. The binned B^0-mass distributions of these two samples are fitted simultaneously in order to determine the sample compositions. The mass distributions span the range 5090–6000 MeV/c^2 and are shown in figure 1 with fit projections overlaid.

The mass distribution of B^0 candidates in the pion-like sample features a peak at the known B^0 mass with a width of about 20 MeV/c^2, corresponding to $B^0 \to D^\mp \pi^\pm$

JHEP06(2018)084

signal decays, and is modelled with the sum of a double-sided Hypatia function [29] and a Johnson SU function [30]. The combinatorial background is modelled using the sum of two exponential functions. At values lower than 5.2 GeV/c^2, broad structures corresponding to partially reconstructed decays, such as $B^0 \to D^-\rho^+(\to \pi^+\pi^0)$, $B^- \to D^-\rho^0(\to \pi^+\pi^-)$ and $B^0 \to D^{*-}(\to D^-\pi^0)\pi^+$ where the additional pion is not reconstructed, are present; the shapes of these backgrounds are determined from simulation. Cross-feed $B^0 \to D^\mp K^\pm$ decays, due to kaon-to-pion misidentification, contaminating the left tail of the signal peak, are described with a double-sided Hypatia function with parameters determined from simulated decays.

The B^0-mass distribution of the kaon-like sample contains analogous components: the $B^0 \to D^\mp K^\pm$ signal peak is modelled with a single-sided Hypatia function; the combinatorial background with an exponential function; partially reconstructed $B^0 \to D^-\rho^+(\to \pi^+\pi^0)$, $B^0 \to D^{*-}(\to D^-\pi^0)\pi^+$, $B^0 \to D^{*-}(\to D^-\pi^0)K^+$ and $B^0 \to D^-K^{*+}(\to \pi^0K^+)$ decays, where the charged pion is misidentified as a kaon and the neutral pion is not reconstructed, are modelled using simulation. Cross-feed $B^0 \to D^\mp\pi^\pm$ decays from pion-to-kaon misidentification in the kaon-like sample peaks to the right of the $B^0 \to D^\mp K^\pm$ signal region, with a long tail towards the high-mass region; the shape of this distribution, a double-sided Hypatia function, is taken from simulation.

The yields of all components are floating parameters of the fit. The yield of the $B^0 \to D^\mp K^\pm$ cross-feed decays in the pion-like sample is constrained to that of the $B^0 \to D^\mp K^\pm$ signal decays in the kaon-like sample using the kaon-to-pion misidentification probability and the kaon identification efficiency of the PID requirement on the companion particle. In a similar manner, the yield of the $B^0 \to D^\mp\pi^\pm$ cross-feed decays in the kaon-like sample is constrained to that of $B^0 \to D^\mp\pi^\pm$ signal decays in the pion-like sample scaled by the pion-to-kaon misidentification probability and the pion identification efficiency. The misidentification probabilities and the identification efficiencies are determined from a large sample of $D^{*+} \to D^0(\to K^-\pi^+)\pi^+$ decays in which the charged tracks are weighted in momentum and pseudorapidity to match those of the companion particle in $B^0 \to D^\mp\pi^\pm$ decays [31].

An unbinned maximum-likelihood fit to the B^0-mass distribution of the pion-like sample is performed to determine *sWeights* [32], which are used to statistically subtract the background in the decay-time analysis of section 6. This unbinned fit contains the same components as the binned fit, but applied in a smaller mass window, 5220–5600 MeV/c^2, to suppress the background contamination. All backgrounds entering this mass region are combined to form a single shape according to the fractions found in the previous fit. The shape parameters of the signal and background components are also fixed to the values found in the preceding fit. The $B^0 \to D^\mp\pi^\pm$ signal yield is found to be $479\,000 \pm 700$ and that of the background to be $34\,400 \pm 300$.

5 Flavour tagging

A combination of tagging algorithms is used to determine the flavour of the B^0 candidates at production. Each algorithm provides a decision (tag), d, which determines the flavour,

JHEP06(2018)084

and an estimate, η, of the probability that the decision is incorrect (mistag probability). The decision takes the value of $d = 1$ for a candidate tagged as a B^0, and $d = -1$ for a candidate tagged as $\overline{B}^0$. The mistag probability is defined only between 0 and 0.5, since $\eta > 0.5$ corresponds to an opposite tag with a mistag probability of $(1 - \eta)$.

Two classes of flavour tagging algorithms are used: opposite-side, OS, and same-side, SS, taggers. The OS tagger exploits the dominant production mechanism of b hadrons, the incoherent production of $b\bar{b}$ pairs, by identifying signatures of the b hadron produced together with the signal B^0 meson. The time evolution of the signal B^0 meson is independent from that of the accompanying b hadron. The OS tagger uses the charge of the electron or muon from semileptonic b-hadron decays, the charge of the kaon from a $b \to c \to s$ decay chain, the charge of a reconstructed secondary charm hadron, and the charge of particles associated with a secondary vertex distinct from the signal decay; further details are given in refs. [33, 34].

The SS tagger selects pions and protons related to the hadronisation process of the signal B^0 meson by means of BDT classifiers that determine the tag decision and mistag probability, as described in ref. [35]. Unlike ref. [35], where $B^0 \to D^{\mp}\pi^{\pm}$ decays are used assuming $S_f = S_{\bar{f}} = 0$, the BDT classifiers of the SS algorithm exploited in this analysis are trained on a control sample of flavour-specific $B^0 \to J/\psi K^{*0}$ decays, whose distributions of p_{T}, pseudorapidity, azimuthal angle of the B^0 candidate, as well as number of tracks and PVs in the event, are weighted to match those of the $B^0 \to D^{\mp}\pi^{\pm}$ signal decay.

Around 37% of the B^0 candidates are tagged by the OS tagger, 79% by the SS tagger, and 31% by both algorithms. About 15% of the B^0 candidates are not tagged by either of the algorithms and are discarded. Each tagging decision is weighted by the estimated mistag probability η, which dilutes the sensitivity to the *CP* asymmetry. To correct for potential biases in η, a function $\omega(\eta)$ is used to calibrate the mistag probability which provides an unbiased estimate of the mistag fraction ω ($\bar{\omega}$), i.e. the fraction of incorrectly tagged candidates for a B^0 ($\overline{B}^0$) meson, for any value of η.

Charged particles used for flavour tagging, such as the kaons from the $b \to c \to s$ decay chain exploited in the OS tagger, can have different interaction cross-sections with the detector material and therefore different reconstruction efficiencies. This can result in different tagging efficiencies and mistag probabilities for initial B^0 and $\overline{B}^0$ mesons. Asymmetries in the tagging efficiency are found to be consistent with zero in simulation and data for both taggers and are therefore neglected in the baseline fit, but considered as a source of systematic uncertainty. This is not the case for the asymmetries of the mistag probability, which can bias the determination of the *CP* asymmetries and must be corrected for. Therefore, the calibration functions depend on the initial flavour of the B^0 candidate: $\omega(\eta)$ for $d = +1$ and $\overline{\omega}(\eta)$ for $d = -1$. They are expressed as generalised linear models (GLMs) of the form

$$\overset{(-)}{\omega}(\eta) = g\big(h(\eta)\big) = g\left(g^{-1}(\eta) + \sum_{i=1}^{N}\left(p_i \overset{(-)}{+} \frac{\Delta p_i}{2}\right) f_i(\eta)\right), \tag{5.1}$$

where p_i and Δp_i are free parameters, f_i are the *basis functions*, and g is the *link function* [36].

JHEP06(2018)084

The calibration function of the OS tagger is a GLM using natural splines as the basis functions [37] with five *knots*, $N = 5$. For the SS tagger, a GLM using first-order polynomial basis functions and $N = 2$ is used. In both cases a modified logistic function, $g(x) = \frac{1}{2}(1 + e^x)^{-1}$, is used as the link function. To account for the tagging decision and mistag probability, the following substitutions occur in eq. (1.1):

$$\begin{aligned} S_f &\to (\Delta^- - \Delta^+) S_f \,, \\ C_f &\to (\Delta^- - \Delta^+) C_f \,. \end{aligned} \tag{5.2}$$

Similar equations hold for $S_{\bar{f}}$ and $C_{\bar{f}}$. The calibration functions enter the coefficients $\Delta^\pm$ along with the tagging efficiencies $\varepsilon_{\rm OS}$ and $\varepsilon_{\rm SS}$ of the OS and SS taggers, according to

$$\begin{aligned} \Delta^\pm = &\frac{1}{2}\varepsilon_{\rm OS}\left[1 - \varepsilon_{\rm SS} + d_{\rm OS}\Big(1 - \varepsilon_{\rm SS} - 2\omega(\eta_{\rm OS})\big(1 + \varepsilon_{\rm SS}\big)\Big)\right] \\ &\pm \frac{1}{2}\varepsilon_{\rm OS}\left[1 - \varepsilon_{\rm SS} + d_{\rm OS}\Big(1 - \varepsilon_{\rm SS} - 2\overline{\omega}(\eta_{\rm OS})\big(1 + \varepsilon_{\rm SS}\big)\Big)\right], \end{aligned} \tag{5.3}$$

for candidates tagged by the OS algorithm and not by the SS algorithm (and vice-versa, exchanging the OS and SS indexes), and

$$\begin{aligned} \Delta^\pm = &\frac{1}{4}\varepsilon_{\rm OS}\varepsilon_{\rm SS}\left[1 + \sum_{j={\rm OS,SS}} d_j\Big(1 - 2\omega(\eta_j)\Big) + d_{\rm OS}d_{\rm SS}\Big(1 - 2\omega(\eta_j) + 2\omega(\eta_{\rm OS})\omega(\eta_{\rm SS})\Big)\right] \\ &\pm \frac{1}{4}\varepsilon_{\rm OS}\varepsilon_{\rm SS}\left[1 + \sum_{j={\rm OS,SS}} d_j\Big(1 - 2\overline{\omega}(\eta_j)\Big) + d_{\rm OS}d_{\rm SS}\Big(1 - 2\overline{\omega}(\eta_j) + 2\overline{\omega}(\eta_{\rm OS})\overline{\omega}(\eta_{\rm SS})\Big)\right], \end{aligned} \tag{5.4}$$

for candidates tagged by both algorithms. The form of the $\Delta^\pm$ coefficients and of the substitutions of eq. (5.2) is convenient to also account for other spurious asymmetries considered in section 6.

The seven pairs of calibration parameters $(p_i, \Delta p_i)$ are left free in the fit from which the S_f and $S_{\bar{f}}$ observables are extracted. This is possible because the C_f and $C_{\bar{f}}$ coefficients are fixed parameters, so that the cosine terms of the decay rates permit the calibration parameters to be measured. This procedure has been validated with pseudoexperiments and possible deviations of C_f and $C_{\bar{f}}$ from unity are taken into account in the systematic uncertainties. To account for possible mismodelling of the calibration functions, systematic uncertainties are assigned to S_f and $S_{\bar{f}}$. The calibration functions obtained in the data are shown in figure 2, where the measured mistag fraction is presented as a function of the predicted mistag probability of the tagger.

Considering only candidates retained for the analysis, i.e. those with a flavour tag, the statistical uncertainties of S_f and $S_{\bar{f}}$ are inversely proportional to $\sqrt{\langle \mathcal{D}^2 \rangle}$. Here, $\langle \mathcal{D}^2 \rangle$ is the average of the squared dilution of the signal, calculated as $\frac{1}{\mathcal{N}_{\rm tag}} \sum_{i=1}^{N_{\rm tag}} w_i \left[1 - 2\omega(\eta_i)\right]^2$, where $N_{\rm tag}$ is the number of candidates, w_i is the *sWeight* of the candidate i determined in the fit of the sample composition, and $\mathcal{N}_{\rm tag} = \sum_{i=1}^{N_{\rm tag}} w_i$. The total dilution squared of the sample is found to be $(6.554 \pm 0.017)\%$. Considering also the number of discarded candidates because no tagging decision is determined by either tagger, $N_{\rm untag}$ and $\mathcal{N}_{\rm untag} = \sum_{i=1}^{N_{\rm untag}} w_i$, the tagging efficiency $\varepsilon_{\rm tag} \equiv \mathcal{N}_{\rm tag}/(\mathcal{N}_{\rm tag} + \mathcal{N}_{\rm untag})$ is found to be $(85.23 \pm 0.05)\%$. Hence,

JHEP06(2018)084

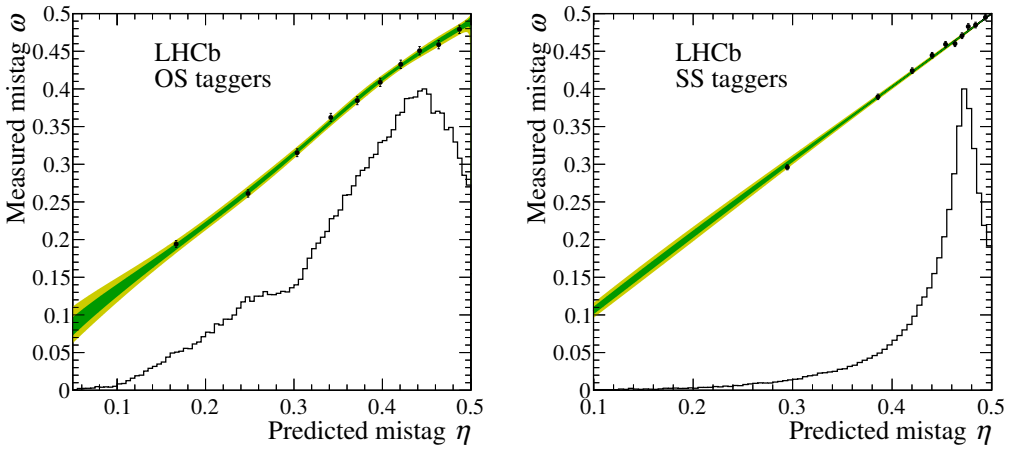

Figure 2. Measured mistag fraction ω versus predicted mistag probability η of the combination of (left) OS and (right) SS taggers as determined in signal decays with the fit described in section 6. The black histograms are the distributions of the mistag probabilities in arbitrary units. The shaded areas correspond to the 68% and 95% confidence-level regions of the calibration functions and do not include systematic uncertainties on the parameters. The calibration functions and the distributions of mistag probabilities are shown summing over candidates tagged as either B^0 or $\overline{B}^0$.

the effective tagging efficiency of the initial sample is $\varepsilon_{\rm tag}\langle\mathcal{D}^2\rangle = (5.59\pm0.01)\%$. All quoted uncertainties are statistical only. The effective tagging efficiency is similar to that of the measurement of *CP* violation in $B^0_s \to D^{\mp}_s K^{\pm}$ decays [38].

6 Decay-time fit

The *CP* asymmetries S_f and $S_{\bar{f}}$ are determined from a multidimensional maximum-likelihood fit to the unbinned distributions of the signal candidates weighted with the *sWeights*. The probability density function (PDF) describing the signal decay to a final state F equal to f or $\bar{f}$, at the reconstructed decay time t, and given the tags $\vec{d} = (d_{\rm OS}, d_{\rm SS})$ and mistag probabilities $\vec{\eta} = (\eta_{\rm OS}, \eta_{\rm SS})$, is

$$P(t, F, \vec{d}\,|\,\vec{\eta}) \propto \epsilon(t)\left(\mathcal{P}(t', F, \vec{d}\,|\,\vec{\eta}) \otimes \mathcal{R}(t'-t)\right), \tag{6.1}$$

where $\mathcal{P}(t', F, \vec{d}|\vec{\eta})$ is the function describing the distribution of true decay times t', $\mathcal{R}(t'-t)$ is the decay time resolution, and $\epsilon(t)$ describes the decay-time-dependent efficiency of reconstructing and selecting the signal decays. The function $\mathcal{P}(t', F, \vec{d}\,|\,\vec{\eta})$ corresponds to one of the decay rates of eq. (1.1), according to the final state F, and with the substitutions of eq. (5.2) to include the flavour tagging.

A production asymmetry, $A_{\rm P}$, and a final-state detection asymmetry, $A_{\rm D}$, must also be taken into account. These are defined as

$$A_{\rm P} = \frac{\sigma(\overline{B}^0) - \sigma(B^0)}{\sigma(\overline{B}^0) + \sigma(B^0)}, \qquad A_{\rm D} = \frac{\varepsilon(f) - \varepsilon(\bar{f})}{\varepsilon(f) + \varepsilon(\bar{f})}, \tag{6.2}$$

where ε is the decay-time-integrated efficiency in reconstructing and selecting the final state $\bar{f}$ or f, and σ is the production cross-section of the given $\overline{B}^0$ or B^0 meson. The

JHEP06(2018)084

asymmetry $A_{\rm P}$ arises from the different production cross-sections of $\overline{B}^0$ and B^0 mesons in proton-proton collisions and is measured to be at the percent level at LHC energies [39]. The detection asymmetry is also measured to be at the percent level and to be independent of the decay time. Therefore, eq. (5.2) is further modified as follows:

$$\begin{aligned}(\Delta^- - \Delta^+)S_f &\to (\Delta^- - A_{\rm P}\Delta^+)(1 + A_{\rm D})S_f\,,\\ (\Delta^- - \Delta^+)C_f &\to (\Delta^- - A_{\rm P}\Delta^+)(1 + A_{\rm D})C_f\,,\end{aligned} \tag{6.3}$$

where C_f is fixed to 1. Similar equations hold for $S_{\bar{f}}$ and $C_{\bar{f}}$ (fixed to -1) with $A_{\rm D} \to -A_{\rm D}$.

The decay-time resolution is determined from a sample of *fake* B^0 candidates formed from a genuine D^- meson and a charged track originating from the same PV and consistent with being a pion of opposite charge. These candidates are subjected to a selection similar to that of the signal decays except for all decay-time biasing requirements, which are removed. The decay-time distribution of these candidates is therefore expected to peak at zero with a Gaussian shape given by the resolution function. Its width is determined in bins of the uncertainty on the decay time provided by the kinematic fit of the decay chain. A second-order polynomial is used to describe the measured width as a function of the decay-time uncertainty. The average resolution of (54.9 ± 0.4) fs is used as the width of the Gaussian resolution function $\mathcal{R}(t' - t)$. The efficiency function $\epsilon(t)$ is modelled by segments of cubic b-splines [40] with nine free parameters in total.

The free parameters of the fit are the S_f and $S_{\bar{f}}$ coefficients, the detection and production asymmetries $A_{\rm D}$ and $A_{\rm P}$, the seven pairs of parameters $(p_i, \Delta p_i)$ for the calibration functions of the OS and SS taggers, their efficiencies $\varepsilon_{\rm OS}$ and $\varepsilon_{\rm SS}$, and the nine parameters of $\epsilon(t)$. The average B^0 decay width, Γ in eq. (1.1), is constrained by means of a Gaussian function whose mean is the world average value and whose width is the uncertainty [6]. Similarly, the B^0–$\overline{B}^0$ mixing frequency, Δm, is constrained to the value measured in ref. [41].

The fit determines $S_f = 0.058 \pm 0.021$ and $S_{\bar{f}} = 0.038 \pm 0.021$ where the uncertainties include the contributions from the constraints on the decay width and mixing frequency. When the fit is repeated by fixing Δm and Γ to the central values used in the constraints, the central values for S_f and $S_{\bar{f}}$ do not change and their uncertainties decrease to 0.020. This is considered as the statistical uncertainty for both S_f and $S_{\bar{f}}$. The statistical correlation between S_f and $S_{\bar{f}}$ is 60%. This correlation is introduced by the flavour tagging and by the production asymmetry. The distribution of the decay time with the overlaid projection of the fit is shown in figure 3.

The values reported for S_f and $S_{\bar{f}}$ result in a significance of 2.7σ for the *CP*-violation hypothesis, according to Wilks' theorem. Figure 4 reports the decay-time-dependent signal-yield asymmetries between candidates tagged as B^0 and $\overline{B}^0$, for the decays split according to the favoured (F) $\bar{b} \to \bar{c}u\bar{d}$ and the suppressed (S) $\bar{b} \to \bar{u}c\bar{d}$ transitions

$$A_{\rm F} = \frac{\Gamma_{B^0\to f}(t) - \Gamma_{\overline{B}^0\to \bar{f}}(t)}{\Gamma_{B^0\to f}(t) + \Gamma_{\overline{B}^0\to \bar{f}}(t)} \tag{6.4}$$

$$A_{\rm S} = \frac{\Gamma_{\overline{B}^0\to f}(t) - \Gamma_{B^0\to \bar{f}}(t)}{\Gamma_{\overline{B}^0\to f}(t) + \Gamma_{B^0\to \bar{f}}(t)}. \tag{6.5}$$

JHEP06(2018)084

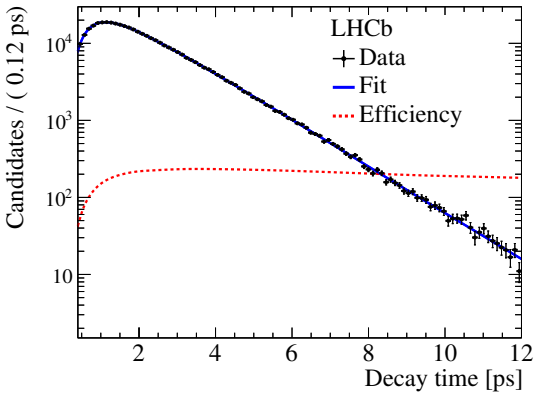

Figure 3. Background-subtracted decay-time distribution for tagged candidates. The solid blue curve is the projection of the signal PDF. The red dotted curve indicates the efficiency function $\varepsilon(t)$ in arbitrary units.

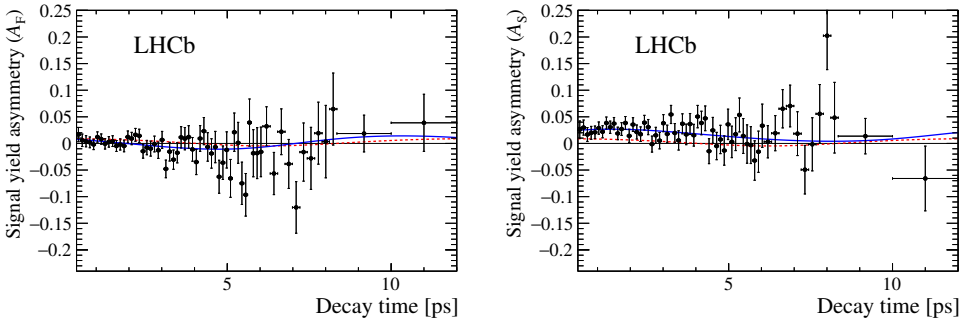

Figure 4. Decay-time-dependent signal-yield asymmetries for (left) the favoured and (right) the suppressed decays. The signal-yield asymmetries are defined in eq. (6.4) and eq. (6.5). The blue solid curve is the projection of the signal PDF, the red dotted curve indicates the projection of the fit when *CP* conservation is imposed.

The fit projections are overlaid to the asymmetries of the data, along with the curves expected when $S_{\bar{f}} = -S_f$ is imposed, i.e. in the hypothesis of no *CP* violation.

Several consistency checks are made by performing the fit on subsets of the data sample split according to different data-taking conditions, tagging algorithms, number of tracks in the event, and trigger requirements. These fits show good agreement with the result presented here. The stability of the result is also analysed in bins of the transverse momentum of the B^0 meson and in bins of the difference of pseudorapidity between the D^- candidate and the companion pion.

The production asymmetry and the detection asymmetry are compared with results of independent LHCb measurements. The values found in this analysis are $A_{\rm P} = (-0.64 \pm 0.28)\%$ and $A_{\rm D} = (0.86 \pm 0.19)\%$, where the uncertainties are statistical, in agreement with those derived from ref. [39], when accounting for the different kinematics of the signals.

The values of the flavour-tagging parameters are also determined in control samples. The $B^+ \to \overline{D}{}^0\pi^+$ decay is used for the OS tagger. As the quarks that accompany the b

JHEP06(2018)084

quark in B^+ and B^0 mesons differ, the SS calibration function is studied with $B^0 \to J/\psi K^{*0}$ decays from a sample that is disjoint to that used in the training of the BDT classifiers. In both cases, distributions of $p_{\rm T}$ and pseudorapidity of the B^0 candidate, number of tracks and PVs in the event, and the composition of software trigger decisions are weighted to match those of the $B^0 \to D^{\mp}\pi^{\pm}$ signal sample. In the case of the $B^+ \to \overline{D}{}^0\pi^+$ mode, the decay-time distribution of the B^+ and D^0 mesons are also weighted to match those of the B^0 and D^- mesons of the signal decays, while in the case of the $B^0 \to J/\psi K^{*0}$ decay the azimuthal angle of the B^0 is weighted to match that of the $B^0 \to D^{\mp}\pi^{\pm}$ signal sample. The charged pion produced in $B^+ \to \overline{D}{}^0\pi^+$ decays directly identifies the B^+ flavour at production. Therefore, the calibration of the OS tagger is achieved by counting the number of correctly and incorrectly tagged signal candidates. In contrast, the SS tagger calibration with $B^0 \to J/\psi K^{*0}$ decays requires the B^0–$\overline{B}{}^0$ flavour oscillations to be resolved by using the decay time as an additional observable, since the amplitude of the observed oscillation is related to the mistag fraction [35]. The values of the calibration parameters found in the control decays are in agreement with those determined in the fit to the signal, with the largest deviation being of 2 standard deviations for two of the Δp_i parameters.

7 Systematic uncertainties

Systematic uncertainties due to external measurements used in the fit are accounted for through Gaussian constraints in the likelihood function. These parameters are the mixing frequency, Δm, and the B^0 decay width, Γ. In order to disentangle these contributions from the statistical uncertainty of S_f and $S_{\bar{f}}$, the fit is repeated by fixing Δm and Γ to the central values used in the constraints. The systematic uncertainty due to the constraint on Γ is found to be negligible, and that due to Δm is 0.0073 and 0.0061 for S_f and $S_{\bar{f}}$, respectively. These are the largest systematic uncertainties of S_f and $S_{\bar{f}}$ and are found to be fully anticorrelated. The correlation of Δm with S_f is -34% and that with $S_{\bar{f}}$ is 29%.

Validation of the entire analysis using ensembles of simulated signal candidates shows that the values of S_f and $S_{\bar{f}}$ are biased up to 0.0068 and 0.0018, respectively. The size of these potential biases are small and so are taken as a systematic uncertainty. The correlation of these systematic uncertainties is 40%.

Variation of the fit to the $D^-\pi^+$ invariant-mass distribution used to calculate the *sWeights* for the background subtraction leads to systematic uncertainties on S_f and $S_{\bar{f}}$ of 0.0042 and 0.0023, respectively. Their correlation is 70%.

The remaining systematic uncertainties are much smaller than those reported above. Hence, the correlation between the systematic uncertainty of S_f and $S_{\bar{f}}$ for the sources that follow are neglected. The systematic uncertainties associated with the PID efficiencies used in the fit to the $D^-\pi^+$ invariant mass are also propagated by means of Gaussian constraints. These uncertainties take into account the size of the calibration samples and the dependence of the results on the binning scheme adopted for weighting the kinematic distributions of the particles of the control decays to match those of the companion tracks. They contribute an uncertainty of 0.0008 to both S_f and $S_{\bar{f}}$.

JHEP06(2018)084

The other sources of systematic uncertainty are calculated by means of pseudoexperiments, where samples of the same size as the data are generated by sampling the PDF with parameters fixed to the value found in data. In the generation of the pseudoexperiments the PDF is modified to consider alternative models according to the source of systematic uncertainty under investigation. The generated sample is then fit with the nominal model. For each parameter, the mean of the distribution of the residuals is considered, $(S_i^{\rm gen} - S_i^{\rm fit})$, from 1000 pseudoexperiments as the systematic uncertainty. If the mean differs from zero by less than one standard deviation, the error on the mean is taken as the systematic uncertainty.

To test the impact of the choice of the calibration models, pseudoexperiments are generated using for the SS calibration the nominal model, while for the OS the degree of the polynomial used in the model is reduced by one unit compared to the nominal model. In the fit for both taggers the degrees of the calibration models are increased by one degree compared to that used to generate the pseudoexperiments. The systematic uncertainties are determined to be 0.0008 and 0.0016 for S_f and $S_{\bar{f}}$, respectively.

Assuming values for the flavour-tagging efficiency asymmetries different from zero, based on what is found in simulation, leads to systematic uncertainties of 0.0012 and 0.0015 for S_f and $S_{\bar{f}}$, respectively.

A different decay-time acceptance model is used in generation by considering new boundaries of the subranges of the spline functions. This results in a systematic uncertainty of 0.0007 for both S_f and $S_{\bar{f}}$.

Mismodelling of the decay-time resolution is also considered by increasing and decreasing the nominal resolution by 20 fs. The largest residuals are considered as the systematic uncertainties, and are 0.0012 and 0.0008 for S_f and $S_{\bar{f}}$, respectively.

A value for $C_f = -C_{\bar{f}}$ different from 1, based on the value of $r_{D\pi}$ from refs. [4, 5] is assumed, resulting in a variation of 0.0006 for both S_f and $S_{\bar{f}}$. By assigning to $\Delta\Gamma$ a value different from zero and equal to the world-average value plus its uncertainty [6] leads to a systematic uncertainty of 0.0007 on both S_f and $S_{\bar{f}}$.

The sources of systematic uncertainties are summarised in table 1. They total 0.011 and 0.007 for S_f and $S_{\bar{f}}$, respectively, with a correlation of -41%.

8 Interpretation of the *CP* asymmetries

The values of S_f and $S_{\bar{f}}$ are interpreted in terms of the angle $2\beta+\gamma$, the ratio of amplitudes $r_{D\pi}$, and the strong phase δ, using the statistical method described in ref. [7].

By taking external measurements of $r_{D\pi}$, confidence intervals for $|\sin(2\beta+\gamma)|$ and δ are derived. The ratio $r_{D\pi}$ is calculated from the branching fraction of $B^0 \to D_s^+\pi^-$ decays, assuming SU(3) symmetry, following the same relation used in refs. [4, 5]:

$$r_{D\pi} = \tan\theta_c \frac{f_{D^+}}{f_{D_s}} \sqrt{\frac{\mathcal{B}(B^0 \to D_s^+\pi^-)}{\mathcal{B}(B^0 \to D^-\pi^+)}}, \tag{8.1}$$

where $\tan\theta_c = 0.23101 \pm 0.00032$ is the tangent of the Cabibbo angle from ref. [42], $f_{D_s}/f_{D^+} = 1.173 \pm 0.003$ is the ratio of decay constants [43–45], and

Source	S_f	$S_{\bar{f}}$
uncertainty of Δm	0.0073	0.0061
fit biases	0.0068	0.0018
background subtraction	0.0042	0.0023
PID efficiencies	0.0008	0.0008
flavour-tagging models	0.0011	0.0015
flavour-tagging efficiency asymmetries	0.0012	0.0015
$\epsilon(t)$ model	0.0007	0.0007
assumption on $\Delta\Gamma$	0.0007	0.0007
decay-time resolution	0.0012	0.0008
assumption on C	0.0006	0.0006
total	0.0111	0.0073
statistical uncertainty	0.0198	0.0199

Table 1. Systematic uncertainties on the *CP* asymmetries S_f and $S_{\bar{f}}$. The total uncertainty is the sum in quadrature of the individual contributions.

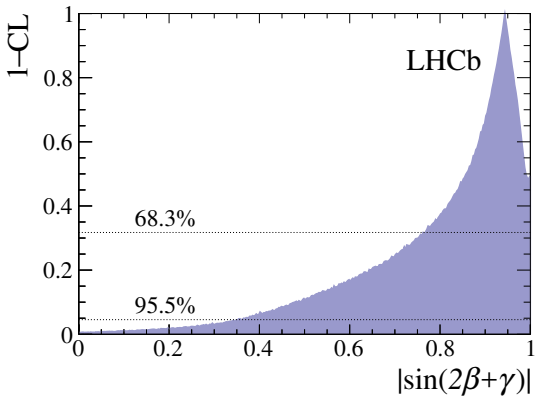

Figure 5. 1–CL as a function of $|\sin(2\beta+\gamma)|$.

$\mathcal{B}(B^0 \to D_s^+\pi^-) = (2.16 \pm 0.26) \times 10^{-5}$ and $\mathcal{B}(B^0 \to D^-\pi^+) = (2.52 \pm 0.13) \times 10^{-3}$ are branching fractions taken from ref. [25]. We determine $r_{D\pi} = 0.0182 \pm 0.0012 \pm 0.0036$, where the second uncertainty accounts for possible nonfactorizable SU(3)-breaking effects, considered to be 20% of the value of $r_{D\pi}$ as suggested in ref. [46]. In addition, using the known value of $\beta = (22.2 \pm 0.7)^\circ$ [6], confidence intervals for γ are determined.

The confidence intervals are

$$\begin{aligned} |\sin(2\beta+\gamma)| &\in [0.77, 1.0]\,, \\ \gamma &\in [5, 86]^\circ \cup [185, 266]^\circ\,, \\ \delta &\in [-41, 41]^\circ \cup [140, 220]^\circ\,, \end{aligned}$$

all at the 68% confidence level (CL). The uncertainties on $r_{D\pi}$ and β have a negligible impact on these values. The intervals are illustrated in figures 5 and 6.

JHEP06(2018)084

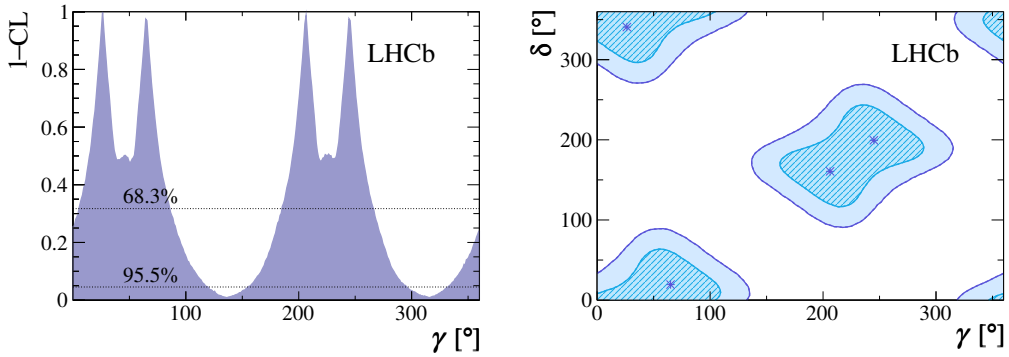

Figure 6. (Left) 1–CL as a function of γ and (right) confidence regions for γ and δ. The confidence regions hold the 39% and 87% CL. Points denote the preferred values.

9 Conclusion

A measurement of the *CP* asymmetries S_f and $S_{\bar{f}}$ in the decay $B^0 \to D^{\mp}\pi^{\pm}$ is reported. The decay candidates are reconstructed in a data set collected with the LHCb experiment at centre-of-mass energies of 7 and 8 TeV, corresponding to an integrated luminosity of $3.0\,\text{fb}^{-1}$. We measure

$$S_f = 0.058 \pm 0.020\,(\text{stat}) \pm 0.011\,(\text{syst}),$$
$$S_{\bar{f}} = 0.038 \pm 0.020\,(\text{stat}) \pm 0.007\,(\text{syst}),$$

with a correlation of 60% (−41%) between the statistical (systematic) uncertainties. These values are in agreement with, and more precise than, measurements from the Belle and BaBar collaborations [9, 10]. This measurement, in combination with the external inputs of $r_{D\pi}$ and β, constrains the CKM angle γ to be in the interval $[5, 86]^\circ \cup [185, 266]^\circ$ at the 68% confidence level.

Acknowledgments

We express our gratitude to our colleagues in the CERN accelerator departments for the excellent performance of the LHC. We thank the technical and administrative staff at the LHCb institutes. We acknowledge support from CERN and from the national agencies: CAPES, CNPq, FAPERJ and FINEP (Brazil); MOST and NSFC (China); CNRS/IN2P3 (France); BMBF, DFG and MPG (Germany); INFN (Italy); NWO (The Netherlands); MNiSW and NCN (Poland); MEN/IFA (Romania); MinES and FASO (Russia); MinECo (Spain); SNSF and SER (Switzerland); NASU (Ukraine); STFC (United Kingdom); NSF (U.S.A.). We acknowledge the computing resources that are provided by CERN, IN2P3 (France), KIT and DESY (Germany), INFN (Italy), SURF (The Netherlands), PIC (Spain), GridPP (United Kingdom), RRCKI and Yandex LLC (Russia), CSCS (Switzerland), IFIN-HH (Romania), CBPF (Brazil), PL-GRID (Poland) and OSC (U.S.A.). We are indebted to the communities behind the multiple open-source software packages on which we depend. Individual groups or members have received support from AvH Foundation

JHEP06(2018)084

(Germany), EPLANET, Marie Skłodowska-Curie Actions and ERC (European Union), ANR, Labex P2IO and OCEVU, and Région Auvergne-Rhône-Alpes (France), Key Research Program of Frontier Sciences of CAS, CAS PIFI, and the Thousand Talents Program (China), RFBR, RSF and Yandex LLC (Russia), GVA, XuntaGal and GENCAT (Spain), Herchel Smith Fund, the Royal Society, the English-Speaking Union and the Leverhulme Trust (United Kingdom).

JHEP06(2018)084

References

[1] I. Dunietz and R.G. Sachs, *Asymmetry between inclusive charmed and anticharmed modes in B^0, $\bar{B}^0$ decay as a measure of CP violation*, *Phys. Rev.* **D 37** (1988) 3186 [*Erratum ibid.* **D 39** (1989) 3515] [INSPIRE].

[2] R. Aleksan, I. Dunietz and B. Kayser, *Determining the CP-violating phase γ*, *Z. Phys.* **C 54** (1992) 653 [INSPIRE].

[3] R. Fleischer, *New strategies to obtain insights into CP-violation through $B_{(s)} \to D^{\pm}_{(s)} K^{\mp}$, $D^{*\pm}_{(s)} K^{\mp}$, ... and $B_{(d)} \to D^{\pm}\pi^{\mp}$, $D^{*\pm}\pi^{\mp}$, ... decays*, *Nucl. Phys.* **B 671** (2003) 459 [hep-ph/0304027] [INSPIRE].

[4] BaBar collaboration, B. Aubert et al., *Measurement of the Branching Fractions of the Rare Decays $B^0 \to D_s^{(*)+}\pi^-$, $B^0 \to D_s^{(*)+}\rho^-$ and $B^0 \to D_s^{(*)-}K^{(*)+}$*, *Phys. Rev.* **D 78** (2008) 032005 [arXiv:0803.4296] [INSPIRE].

[5] Belle collaboration, A. Das et al., *Measurements of branching fractions for $B^0 \to D_s^+\pi^-$ and $\bar{B}^0 \to D_s^+K^-$*, *Phys. Rev.* **D 82** (2010) 051103 [arXiv:1007.4619] [INSPIRE].

[6] HFLAV collaboration, Y. Amhis et al., *Averages of b-hadron, c-hadron and τ-lepton properties as of summer 2016*, *Eur. Phys. J.* **C 77** (2017) 895 [arXiv:1612.07233] [INSPIRE].

[7] LHCb collaboration, *Measurement of the CKM angle γ from a combination of LHCb results*, *JHEP* **12** (2016) 087 [arXiv:1611.03076] [INSPIRE].

[8] BaBar collaboration, B. Aubert et al., *Measurement of time-dependent CP-violating asymmetries and constraints on $\sin(2\beta+\gamma)$ with partial reconstruction of $B \to D^{*\mp}\pi^{\pm}$ decays*, *Phys. Rev.* **D 71** (2005) 112003 [hep-ex/0504035] [INSPIRE].

[9] BaBar collaboration, B. Aubert et al., *Measurement of time-dependent CP asymmetries in $B^0 \to D^{(*)\pm}\pi^{\mp}$ and $B^0 \to D^{\pm}\rho^{\mp}$ decays*, *Phys. Rev.* **D 73** (2006) 111101 [hep-ex/0602049] [INSPIRE].

[10] Belle collaboration, F.J. Ronga et al., *Measurements of CP-violation in $B^0 \to D^{*-}\pi^+$ and $B^0 \to D^-\pi^+$ decays*, *Phys. Rev.* **D 73** (2006) 092003 [hep-ex/0604013] [INSPIRE].

[11] Belle collaboration, S. Bahinipati et al., *Measurements of time-dependent CP asymmetries in $B \to D^{*\mp}\pi^{\pm}$ decays using a partial reconstruction technique*, *Phys. Rev.* **D 84** (2011) 021101 [arXiv:1102.0888] [INSPIRE].

[12] LHCb collaboration, *The LHCb Detector at the LHC*, 2008 *JINST* **3** S08005 [INSPIRE].

[13] LHCb collaboration, *LHCb detector performance*, *Int. J. Mod. Phys.* **A 30** (2015) 1530022 [arXiv:1412.6352] [INSPIRE].

[14] R. Aaij et al., *Performance of the LHCb vertex locator*, 2014 *JINST* **9** P09007 [arXiv:1405.7808] [INSPIRE].

[15] LHCb Outer Tracker Group collaboration, *Performance of the LHCb Outer Tracker*, 2014 *JINST* **9** P01002 [arXiv:1311.3893] [INSPIRE].

[16] T. Sjöstrand, S. Mrenna and P.Z. Skands, *PYTHIA 6.4 physics and manual*, *JHEP* **05** (2006) 026 [hep-ph/0603175] [INSPIRE].

[17] T. Sjöstrand, S. Mrenna and P.Z. Skands, *A brief introduction to PYTHIA 8.1*, *Comput. Phys. Commun.* **178** (2008) 852 [arXiv:0710.3820] [INSPIRE].

[18] I. Belyaev et al., *Handling of the generation of primary events in Gauss, the LHCb simulation framework*, *J. Phys. Conf. Ser.* **331** (2011) 032047 [INSPIRE].

[19] D.J. Lange, *The EvtGen particle decay simulation package*, *Nucl. Instrum. Meth.* **A 462** (2001) 152 [INSPIRE].

[20] P. Golonka and Z. Was, *PHOTOS Monte Carlo: a precision tool for QED corrections in Z and W decays*, *Eur. Phys. J.* **C 45** (2006) 97 [hep-ph/0506026] [INSPIRE].

[21] GEANT4 collaboration, J. Allison et al., *Geant4 developments and applications*, *IEEE Trans. Nucl. Sci.* **53** (2006) 270.

[22] GEANT4 collaboration, S. Agostinelli et al., *GEANT4: a simulation toolkit*, *Nucl. Instrum. Meth.* **A 506** (2003) 250 [INSPIRE].

[23] LHCb collaboration, *The LHCb simulation application, Gauss: Design, evolution and experience*, *J. Phys. Conf. Ser.* **331** (2011) 032023 [INSPIRE].

[24] V.V. Gligorov and M. Williams, *Efficient, reliable and fast high-level triggering using a bonsai boosted decision tree*, 2013 *JINST* **8** P02013 [arXiv:1210.6861] [INSPIRE].

[25] Particle Data Group collaboration, C. Patrignani et al., *Review of particle physics*, *Chin. Phys.* **C 40** (2016) 100001 [INSPIRE].

[26] W.D. Hulsbergen, *Decay chain fitting with a Kalman filter*, *Nucl. Instrum. Meth.* **A 552** (2005) 566 [physics/0503191] [INSPIRE].

[27] L. Breiman et al., *Classification and regression trees*, Wadsworth international group, Belmont U.S.A. (1984).

[28] Y. Freund and R.E. Schapire, *A decision-theoretic generalization of on-line learning and an application to boosting*, *J. Comput. Syst. Sci.* **55** (1997) 119.

[29] D. Martínez Santos and F. Dupertuis, *Mass distributions marginalized over per-event errors*, *Nucl. Instrum. Meth.* **A 764** (2014) 150 [arXiv:1312.5000] [INSPIRE].

[30] N.L. Johnson, *Systems of frequency curves generated by methods of translation*, *Biometrika* **36** (1949) 149.

[31] L. Anderlini et al., *The PIDCalib package*, LHCb-PUB-2016-021 (2016).

[32] M. Pivk and F.R. Le Diberder, *SPlot: a statistical tool to unfold data distributions*, *Nucl. Instrum. Meth.* **A 555** (2005) 356 [physics/0402083] [INSPIRE].

[33] LHCb collaboration, *Opposite-side flavour tagging of B mesons at the LHCb experiment*, *Eur. Phys. J.* **C 72** (2012) 2022 [arXiv:1202.4979] [INSPIRE].

JHEP06(2018)084

[34] LHCb collaboration, *B flavour tagging using charm decays at the LHCb experiment*, 2015 *JINST* **10** P10005 [arXiv:1507.07892] [INSPIRE].

[35] LHCb collaboration, *New algorithms for identifying the flavour of* B^0 *mesons using pions and protons*, *Eur. Phys. J.* **C 77** (2017) 238 [arXiv:1610.06019] [INSPIRE].

[36] A. Agresti, *Categorical data analysis*, Wiley Series in Probability and Statistics, U.S.A. (2013).

[37] T. Hastie, R. Tibshirani and J. Friedman, *The elements of statistical learning*, Springer Series in Statistics, Germany (2001).

[38] LHCb collaboration, *Measurement of CP asymmetry in* $B_s^0 \to D_s^{\mp} K^{\pm}$ *decays*, *JHEP* **03** (2018) 059 [arXiv:1712.07428] [INSPIRE].

[39] LHCb collaboration, *Measurement of* B^0, B_s^0, B^+ *and* Λ_b^0 *production asymmetries in* 7 *and* 8 *TeV proton-proton collisions*, *Phys. Lett.* **B 774** (2017) 139 [arXiv:1703.08464] [INSPIRE].

[40] C. de Boor, *A practical guide to splines (revised edition)*, Springer, Germany (2001).

[41] LHCb collaboration, *A precise measurement of the* B^0 *meson oscillation frequency*, *Eur. Phys. J.* **C 76** (2016) 412 [arXiv:1604.03475] [INSPIRE].

[42] CKMFITTER GROUP collaboration, J. Charles et al., *CP violation and the CKM matrix: assessing the impact of the asymmetric B factories*, *Eur. Phys. J.* **C 41** (2005) 1 [hep-ph/0406184] [INSPIRE].

[43] S. Aoki et al., *Review of lattice results concerning low-energy particle physics*, *Eur. Phys. J.* **C 77** (2017) 112 [arXiv:1607.00299] [INSPIRE].

[44] FERMILAB LATTICE, MILC collaboration, A. Bazavov et al., *Charmed and light pseudoscalar meson decay constants from four-flavor lattice QCD with physical light quarks*, *Phys. Rev.* **D 90** (2014) 074509 [arXiv:1407.3772] [INSPIRE].

[45] N. Carrasco et al., *Leptonic decay constants* f_K, f_D, *and* f_{D_s} *with* $N_f = 2 + 1 + 1$ *twisted-mass lattice QCD*, *Phys. Rev.* **D 91** (2015) 054507 [arXiv:1411.7908] [INSPIRE].

[46] K. De Bruyn et al., *Exploring* $B_s \to D_s^{(*)\pm} K^{\mp}$ *decays in the presence of a sizable width difference* $\Delta\Gamma_s$, *Nucl. Phys.* **B 868** (2013) 351 [arXiv:1208.6463] [INSPIRE].

JHEP06(2018)084

The LHCb collaboration

R. Aaij[43], B. Adeva[39], M. Adinolfi[48], Z. Ajaltouni[5], S. Akar[59], P. Albicocco[18], J. Albrecht[10], F. Alessio[40], M. Alexander[53], A. Alfonso Albero[38], S. Ali[43], G. Alkhazov[31], P. Alvarez Cartelle[55], A.A. Alves Jr[59], S. Amato[2], S. Amerio[23], Y. Amhis[7], L. An[3], L. Anderlini[17], G. Andreassi[41], M. Andreotti[16,g], J.E. Andrews[60], R.B. Appleby[56], F. Archilli[43], P. d'Argent[12], J. Arnau Romeu[6], A. Artamonov[37], M. Artuso[61], E. Aslanides[6], M. Atzeni[42], G. Auriemma[26], S. Bachmann[12], J.J. Back[50], S. Baker[55], V. Balagura[7,b], W. Baldini[16], A. Baranov[35], R.J. Barlow[56], S. Barsuk[7], W. Barter[56], F. Baryshnikov[32], V. Batozskaya[29], V. Battista[41], A. Bay[41], J. Beddow[53], F. Bedeschi[24], I. Bediaga[1], A. Beiter[61], L.J. Bel[43], N. Beliy[63], V. Bellee[41], N. Belloli[20,i], K. Belous[37], I. Belyaev[32,40], E. Ben-Haim[8], G. Bencivenni[18], S. Benson[43], S. Beranek[9], A. Berezhnoy[33], R. Bernet[42], D. Berninghoff[12], E. Bertholet[8], A. Bertolin[23], C. Betancourt[42], F. Betti[15,40], M.O. Bettler[49], M. van Beuzekom[43], Ia. Bezshyiko[42], S. Bifani[47], P. Billoir[8], A. Birnkraut[10], A. Bizzeti[17,u], M. Bjørn[57], T. Blake[50], F. Blanc[41], S. Blusk[61], V. Bocci[26], O. Boente Garcia[39], T. Boettcher[58], A. Bondar[36,w], N. Bondar[31], S. Borghi[56,40], M. Borisyak[35], M. Borsato[39,40], F. Bossu[7], M. Boubdir[9], T.J.V. Bowcock[54], E. Bowen[42], C. Bozzi[16,40], S. Braun[12], M. Brodski[40], J. Brodzicka[27], D. Brundu[22], E. Buchanan[48], C. Burr[56], A. Bursche[22], J. Buytaert[40], W. Byczynski[40], S. Cadeddu[22], H. Cai[64], R. Calabrese[16,g], R. Calladine[47], M. Calvi[20,i], M. Calvo Gomez[38,m], A. Camboni[38,m], P. Campana[18], D.H. Campora Perez[40], L. Capriotti[56], A. Carbone[15,e], G. Carboni[25], R. Cardinale[19,h], A. Cardini[22], P. Carniti[20,i], L. Carson[52], K. Carvalho Akiba[2], G. Casse[54], L. Cassina[20], M. Cattaneo[40], G. Cavallero[19,h], R. Cenci[24,p], D. Chamont[7], M.G. Chapman[48], M. Charles[8], Ph. Charpentier[40], G. Chatzikonstantinidis[47], M. Chefdeville[4], S. Chen[22], S.-G. Chitic[40], V. Chobanova[39], M. Chrzaszcz[40], A. Chubykin[31], P. Ciambrone[18], X. Cid Vidal[39], G. Ciezarek[40], P.E.L. Clarke[52], M. Clemencic[40], H.V. Cliff[49], J. Closier[40], V. Coco[40], J. Cogan[6], E. Cogneras[5], V. Cogoni[22,f], L. Cojocariu[30], P. Collins[40], T. Colombo[40], A. Comerma-Montells[12], A. Contu[22], G. Coombs[40], S. Coquereau[38], G. Corti[40], M. Corvo[16,g], C.M. Costa Sobral[50], B. Couturier[40], G.A. Cowan[52], D.C. Craik[58], A. Crocombe[50], M. Cruz Torres[1], R. Currie[52], C. D'Ambrosio[40], F. Da Cunha Marinho[2], C.L. Da Silva[73], E. Dall'Occo[43], J. Dalseno[48], A. Danilina[32], A. Davis[3], O. De Aguiar Francisco[40], K. De Bruyn[40], S. De Capua[56], M. De Cian[41], J.M. De Miranda[1], L. De Paula[2], M. De Serio[14,d], P. De Simone[18], C.T. Dean[53], D. Decamp[4], L. Del Buono[8], B. Delaney[49], H.-P. Dembinski[11], M. Demmer[10], A. Dendek[28], D. Derkach[35], O. Deschamps[5], F. Dettori[54], B. Dey[65], A. Di Canto[40], P. Di Nezza[18], S. Didenko[69], H. Dijkstra[40], F. Dordei[40], M. Dorigo[40], A. Dosil Suárez[39], L. Douglas[53], A. Dovbnya[45], K. Dreimanis[54], L. Dufour[43], G. Dujany[8], P. Durante[40], J.M. Durham[73], D. Dutta[56], R. Dzhelyadin[37], M. Dziewiecki[12], A. Dziurda[40], A. Dzyuba[31], S. Easo[51], U. Egede[55], V. Egorychev[32], S. Eidelman[36,w], S. Eisenhardt[52], U. Eitschberger[10], R. Ekelhof[10], L. Eklund[53], S. Ely[61], A. Ene[30], S. Escher[9], S. Esen[43], H.M. Evans[49], T. Evans[57], A. Falabella[15], N. Farley[47], S. Farry[54], D. Fazzini[20,40,i], L. Federici[25], G. Fernandez[38], P. Fernandez Declara[40], A. Fernandez Prieto[39], F. Ferrari[15], L. Ferreira Lopes[41], F. Ferreira Rodrigues[2], M. Ferro-Luzzi[40], S. Filippov[34], R.A. Fini[14], M. Fiorini[16,g], M. Firlej[28], C. Fitzpatrick[41], T. Fiutowski[28], F. Fleuret[7,b], M. Fontana[22,40], F. Fontanelli[19,h], R. Forty[40], V. Franco Lima[54], M. Frank[40], C. Frei[40], J. Fu[21,q], W. Funk[40], C. Färber[40], E. Gabriel[52], A. Gallas Torreira[39], D. Galli[15,e], S. Gallorini[23], S. Gambetta[52], M. Gandelman[2], P. Gandini[21], Y. Gao[3], L.M. Garcia Martin[71], B. Garcia Plana[39], J. García Pardiñas[42], J. Garra Tico[49], L. Garrido[38], D. Gascon[38], C. Gaspar[40], L. Gavardi[10], G. Gazzoni[5], D. Gerick[12], E. Gersabeck[56], M. Gersabeck[56], T. Gershon[50], Ph. Ghez[4], S. Gianì[41], V. Gibson[49], O.G. Girard[41], L. Giubega[30], K. Gizdov[52], V.V. Gligorov[8], D. Golubkov[32], A. Golutvin[55,69], A. Gomes[1,a], I.V. Gorelov[33], C. Gotti[20,i], E. Govorkova[43], J.P. Grabowski[12],

JHEP06(2018)084

R. Graciani Diaz[38], L.A. Granado Cardoso[40], E. Graugés[38], E. Graverini[42], G. Graziani[17], A. Grecu[30], R. Greim[43], P. Griffith[22], L. Grillo[56], L. Gruber[40], B.R. Gruberg Cazon[57], O. Grünberg[67], E. Gushchin[34], Yu. Guz[37,40], T. Gys[40], C. Göbel[62], T. Hadavizadeh[57], C. Hadjivasiliou[5], G. Haefeli[41], C. Haen[40], S.C. Haines[49], B. Hamilton[60], X. Han[12], T.H. Hancock[57], S. Hansmann-Menzemer[12], N. Harnew[57], S.T. Harnew[48], C. Hasse[40], M. Hatch[40], J. He[63], M. Hecker[55], K. Heinicke[10], A. Heister[9], K. Hennessy[54], L. Henry[71], E. van Herwijnen[40], M. Heß[67], A. Hicheur[2], D. Hill[57], P.H. Hopchev[41], W. Hu[65], W. Huang[63], Z.C. Huard[59], W. Hulsbergen[43], T. Humair[55], M. Hushchyn[35], D. Hutchcroft[54], P. Ibis[10], M. Idzik[28], P. Ilten[47], K. Ivshin[31], R. Jacobsson[40], J. Jalocha[57], E. Jans[43], A. Jawahery[60], F. Jiang[3], M. John[57], D. Johnson[40], C.R. Jones[49], C. Joram[40], B. Jost[40], N. Jurik[57], S. Kandybei[45], M. Karacson[40], J.M. Kariuki[48], S. Karodia[53], N. Kazeev[35], M. Kecke[12], F. Keizer[49], M. Kelsey[61], M. Kenzie[49], T. Ketel[44], E. Khairullin[35], B. Khanji[12], C. Khurewathanakul[41], K.E. Kim[61], T. Kirn[9], S. Klaver[18], K. Klimaszewski[29], T. Klimkovich[11], S. Koliiev[46], M. Kolpin[12], R. Kopecna[12], P. Koppenburg[43], S. Kotriakhova[31], M. Kozeiha[5], L. Kravchuk[34], M. Kreps[50], F. Kress[55], P. Krokovny[36,w], W. Krupa[28], W. Krzemien[29], W. Kucewicz[27,l], M. Kucharczyk[27], V. Kudryavtsev[36,w], A.K. Kuonen[41], T. Kvaratskheliya[32,40], D. Lacarrere[40], G. Lafferty[56], A. Lai[22], G. Lanfranchi[18], C. Langenbruch[9], T. Latham[50], C. Lazzeroni[47], R. Le Gac[6], A. Leflat[33,40], J. Lefrançois[7], R. Lefèvre[5], F. Lemaitre[40], O. Leroy[6], T. Lesiak[27], B. Leverington[12], P.-R. Li[63], T. Li[3], Z. Li[61], X. Liang[61], T. Likhomanenko[68], R. Lindner[40], F. Lionetto[42], V. Lisovskyi[7], X. Liu[3], D. Loh[50], A. Loi[22], I. Longstaff[53], J.H. Lopes[2], D. Lucchesi[23,o], M. Lucio Martinez[39], A. Lupato[23], E. Luppi[16,g], O. Lupton[40], A. Lusiani[24], X. Lyu[63], F. Machefert[7], F. Maciuc[30], V. Macko[41], P. Mackowiak[10], S. Maddrell-Mander[48], O. Maev[31,40], K. Maguire[56], D. Maisuzenko[31], M.W. Majewski[28], S. Malde[57], B. Malecki[27], A. Malinin[68], T. Maltsev[36,w], G. Manca[22,f], G. Mancinelli[6], D. Marangotto[21,q], J. Maratas[5,v], J.F. Marchand[4], U. Marconi[15], C. Marin Benito[38], M. Marinangeli[41], P. Marino[41], J. Marks[12], G. Martellotti[26], M. Martin[6], M. Martinelli[41], D. Martinez Santos[39], F. Martinez Vidal[71], A. Massafferri[1], R. Matev[40], A. Mathad[50], Z. Mathe[40], C. Matteuzzi[20], A. Mauri[42], E. Maurice[7,b], B. Maurin[41], A. Mazurov[47], M. McCann[55,40], A. McNab[56], R. McNulty[13], J.V. Mead[54], B. Meadows[59], C. Meaux[6], F. Meier[10], N. Meinert[67], D. Melnychuk[29], M. Merk[43], A. Merli[21,q], E. Michielin[23], D.A. Milanes[66], E. Millard[50], M.-N. Minard[4], L. Minzoni[16,g], D.S. Mitzel[12], A. Mogini[8], J. Molina Rodriguez[1,y], T. Mombächer[10], I.A. Monroy[66], S. Monteil[5], M. Morandin[23], G. Morello[18], M.J. Morello[24,t], O. Morgunova[68], J. Moron[28], A.B. Morris[6], R. Mountain[61], F. Muheim[52], M. Mulder[43], D. Müller[40], J. Müller[10], K. Müller[42], V. Müller[10], P. Naik[48], T. Nakada[41], R. Nandakumar[51], A. Nandi[57], I. Nasteva[2], M. Needham[52], N. Neri[21], S. Neubert[12], N. Neufeld[40], M. Neuner[12], T.D. Nguyen[41], C. Nguyen-Mau[41,n], S. Nieswand[9], R. Niet[10], N. Nikitin[33], A. Nogay[68], D.P. O'Hanlon[15], A. Oblakowska-Mucha[28], V. Obraztsov[37], S. Ogilvy[18], R. Oldeman[22,f], C.J.G. Onderwater[72], A. Ossowska[27], J.M. Otalora Goicochea[2], P. Owen[42], A. Oyanguren[71], P.R. Pais[41], A. Palano[14], M. Palutan[18,40], G. Panshin[70], A. Papanestis[51], M. Pappagallo[52], L.L. Pappalardo[16,g], W. Parker[60], C. Parkes[56], G. Passaleva[17,40], A. Pastore[14], M. Patel[55], C. Patrignani[15,e], A. Pearce[40], A. Pellegrino[43], G. Penso[26], M. Pepe Altarelli[40], S. Perazzini[40], D. Pereima[32], P. Perret[5], L. Pescatore[41], K. Petridis[48], A. Petrolini[19,h], A. Petrov[68], M. Petruzzo[21,q], B. Pietrzyk[4], G. Pietrzyk[41], M. Pikies[27], D. Pinci[26], F. Pisani[40], A. Pistone[19,h], A. Piucci[12], V. Placinta[30], S. Playfer[52], M. Plo Casasus[39], F. Polci[8], M. Poli Lener[18], A. Poluektov[50], N. Polukhina[69,c], I. Polyakov[61], E. Polycarpo[2], G.J. Pomery[48], S. Ponce[40], A. Popov[37], D. Popov[11,40], S. Poslavskii[37], C. Potterat[2], E. Price[48], J. Prisciandaro[39], C. Prouve[48], V. Pugatch[46], A. Puig Navarro[42], H. Pullen[57], G. Punzi[24,p], W. Qian[63], J. Qin[63], R. Quagliani[8], B. Quintana[5], B. Rachwal[28], J.H. Rademacker[48], M. Rama[24], M. Ramos Pernas[39], M.S. Rangel[2], F. Ratnikov[35,x], G. Raven[44], M. Ravonel Salzgeber[40], M. Reboud[4], F. Redi[41],

JHEP06(2018)084

S. Reichert[10], A.C. dos Reis[1], C. Remon Alepuz[71], V. Renaudin[7], S. Ricciardi[51], S. Richards[48], K. Rinnert[54], P. Robbe[7], A. Robert[8], A.B. Rodrigues[41], E. Rodrigues[59], J.A. Rodriguez Lopez[66], A. Rogozhnikov[35], S. Roiser[40], A. Rollings[57], V. Romanovskiy[37], A. Romero Vidal[39,40], M. Rotondo[18], T. Ruf[40], J. Ruiz Vidal[71], J.J. Saborido Silva[39], N. Sagidova[31], B. Saitta[22,f], V. Salustino Guimaraes[62], C. Sanchez Mayordomo[71], B. Sanmartin Sedes[39], R. Santacesaria[26], C. Santamarina Rios[39], M. Santimaria[18], E. Santovetti[25,j], G. Sarpis[56], A. Sarti[18,k], C. Satriano[26,s], A. Satta[25], D. Savrina[32,33], S. Schael[9], M. Schellenberg[10], M. Schiller[53], H. Schindler[40], M. Schmelling[11], T. Schmelzer[10], B. Schmidt[40], O. Schneider[41], A. Schopper[40], H.F. Schreiner[59], M. Schubiger[41], M.H. Schune[7], R. Schwemmer[40], B. Sciascia[18], A. Sciubba[26,k], A. Semennikov[32], E.S. Sepulveda[8], A. Sergi[47,40], N. Serra[42], J. Serrano[6], L. Sestini[23], P. Seyfert[40], M. Shapkin[37], Y. Shcheglov[31,†], T. Shears[54], L. Shekhtman[36,w], V. Shevchenko[68], B.G. Siddi[16], R. Silva Coutinho[42], L. Silva de Oliveira[2], G. Simi[23,o], S. Simone[14,d], N. Skidmore[12], T. Skwarnicki[61], I.T. Smith[52], M. Smith[55], l. Soares Lavra[1], M.D. Sokoloff[59], F.J.P. Soler[53], B. Souza De Paula[2], B. Spaan[10], P. Spradlin[53], F. Stagni[40], M. Stahl[12], S. Stahl[40], P. Stefko[41], S. Stefkova[55], O. Steinkamp[42], S. Stemmle[12], O. Stenyakin[37], M. Stepanova[31], H. Stevens[10], S. Stone[61], B. Storaci[42], S. Stracka[24,p], M.E. Stramaglia[41], M. Straticiuc[30], U. Straumann[42], S. Strokov[70], J. Sun[3], L. Sun[64], K. Swientek[28], V. Syropoulos[44], T. Szumlak[28], M. Szymanski[63], S. T'Jampens[4], Z. Tang[3], A. Tayduganov[6], T. Tekampe[10], G. Tellarini[16], F. Teubert[40], E. Thomas[40], J. van Tilburg[43], M.J. Tilley[55], V. Tisserand[5], M. Tobin[41], S. Tolk[40], L. Tomassetti[16,g], D. Tonelli[24], R. Tourinho Jadallah Aoude[1], E. Tournefier[4], M. Traill[53], M.T. Tran[41], M. Tresch[42], A. Trisovic[49], A. Tsaregorodtsev[6], A. Tully[49], N. Tuning[43,40], A. Ukleja[29], A. Usachov[7], A. Ustyuzhanin[35], U. Uwer[12], C. Vacca[22,f], A. Vagner[70], V. Vagnoni[15], A. Valassi[40], S. Valat[40], G. Valenti[15], R. Vazquez Gomez[40], P. Vazquez Regueiro[39], S. Vecchi[16], M. van Veghel[43], J.J. Velthuis[48], M. Veltri[17,r], G. Veneziano[57], A. Venkateswaran[61], T.A. Verlage[9], M. Vernet[5], M. Vesterinen[57], J.V. Viana Barbosa[40], D. Vieira[63], M. Vieites Diaz[39], H. Viemann[67], X. Vilasis-Cardona[38,m], A. Vitkovskiy[43], M. Vitti[49], V. Volkov[33], A. Vollhardt[42], B. Voneki[40], A. Vorobyev[31], V. Vorobyev[36,w], C. Voß[9], J.A. de Vries[43], C. Vázquez Sierra[43], R. Waldi[67], J. Walsh[24], J. Wang[61], M. Wang[3], Y. Wang[65], Z. Wang[42], D.R. Ward[49], H.M. Wark[54], N.K. Watson[47], D. Websdale[55], A. Weiden[42], C. Weisser[58], M. Whitehead[9], J. Wicht[50], G. Wilkinson[57], M. Wilkinson[61], M.R.J. Williams[56], M. Williams[58], T. Williams[47], F.F. Wilson[51,40], J. Wimberley[60], M. Winn[7], J. Wishahi[10], W. Wislicki[29], M. Witek[27], G. Wormser[7], S.A. Wotton[49], K. Wyllie[40], D. Xiao[65], Y. Xie[65], A. Xu[3], M. Xu[65], Q. Xu[63], Z. Xu[3], Z. Xu[4], Z. Yang[3], Z. Yang[60], Y. Yao[61], H. Yin[65], J. Yu[65,aa], X. Yuan[61], O. Yushchenko[37], K.A. Zarebski[47], M. Zavertyaev[11,c], L. Zhang[3], W.C. Zhang[3,z], Y. Zhang[7], A. Zhelezov[12], Y. Zheng[63], X. Zhu[3], V. Zhukov[9,33], J.B. Zonneveld[52], S. Zucchelli[15]

[1] *Centro Brasileiro de Pesquisas Físicas (CBPF), Rio de Janeiro, Brazil*
[2] *Universidade Federal do Rio de Janeiro (UFRJ), Rio de Janeiro, Brazil*
[3] *Center for High Energy Physics, Tsinghua University, Beijing, China*
[4] *Univ. Grenoble Alpes, Univ. Savoie Mont Blanc, CNRS, IN2P3-LAPP, Annecy, France*
[5] *Clermont Université, Université Blaise Pascal, CNRS/IN2P3, LPC, Clermont-Ferrand, France*
[6] *Aix Marseille Univ, CNRS/IN2P3, CPPM, Marseille, France*
[7] *LAL, Univ. Paris-Sud, CNRS/IN2P3, Université Paris-Saclay, Orsay, France*
[8] *LPNHE, Université Pierre et Marie Curie, Université Paris Diderot, CNRS/IN2P3, Paris, France*
[9] *I. Physikalisches Institut, RWTH Aachen University, Aachen, Germany*
[10] *Fakultät Physik, Technische Universität Dortmund, Dortmund, Germany*
[11] *Max-Planck-Institut für Kernphysik (MPIK), Heidelberg, Germany*
[12] *Physikalisches Institut, Ruprecht-Karls-Universität Heidelberg, Heidelberg, Germany*
[13] *School of Physics, University College Dublin, Dublin, Ireland*

JHEP06(2018)084

[14] *INFN Sezione di Bari, Bari, Italy*
[15] *INFN Sezione di Bologna, Bologna, Italy*
[16] *INFN Sezione di Ferrara, Ferrara, Italy*
[17] *INFN Sezione di Firenze, Firenze, Italy*
[18] *INFN Laboratori Nazionali di Frascati, Frascati, Italy*
[19] *INFN Sezione di Genova, Genova, Italy*
[20] *INFN Sezione di Milano-Bicocca, Milano, Italy*
[21] *INFN Sezione di Milano, Milano, Italy*
[22] *INFN Sezione di Cagliari, Monserrato, Italy*
[23] *INFN Sezione di Padova, Padova, Italy*
[24] *INFN Sezione di Pisa, Pisa, Italy*
[25] *INFN Sezione di Roma Tor Vergata, Roma, Italy*
[26] *INFN Sezione di Roma La Sapienza, Roma, Italy*
[27] *Henryk Niewodniczanski Institute of Nuclear Physics Polish Academy of Sciences, Kraków, Poland*
[28] *AGH — University of Science and Technology, Faculty of Physics and Applied Computer Science, Kraków, Poland*
[29] *National Center for Nuclear Research (NCBJ), Warsaw, Poland*
[30] *Horia Hulubei National Institute of Physics and Nuclear Engineering, Bucharest-Magurele, Romania*
[31] *Petersburg Nuclear Physics Institute (PNPI), Gatchina, Russia*
[32] *Institute of Theoretical and Experimental Physics (ITEP), Moscow, Russia*
[33] *Institute of Nuclear Physics, Moscow State University (SINP MSU), Moscow, Russia*
[34] *Institute for Nuclear Research of the Russian Academy of Sciences (INR RAS), Moscow, Russia*
[35] *Yandex School of Data Analysis, Moscow, Russia*
[36] *Budker Institute of Nuclear Physics (SB RAS), Novosibirsk, Russia*
[37] *Institute for High Energy Physics (IHEP), Protvino, Russia*
[38] *ICCUB, Universitat de Barcelona, Barcelona, Spain*
[39] *Instituto Galego de Física de Altas Enerxías (IGFAE), Universidade de Santiago de Compostela, Santiago de Compostela, Spain*
[40] *European Organization for Nuclear Research (CERN), Geneva, Switzerland*
[41] *Institute of Physics, Ecole Polytechnique Fédérale de Lausanne (EPFL), Lausanne, Switzerland*
[42] *Physik-Institut, Universität Zürich, Zürich, Switzerland*
[43] *Nikhef National Institute for Subatomic Physics, Amsterdam, The Netherlands*
[44] *Nikhef National Institute for Subatomic Physics and VU University Amsterdam, Amsterdam, The Netherlands*
[45] *NSC Kharkiv Institute of Physics and Technology (NSC KIPT), Kharkiv, Ukraine*
[46] *Institute for Nuclear Research of the National Academy of Sciences (KINR), Kyiv, Ukraine*
[47] *University of Birmingham, Birmingham, United Kingdom*
[48] *H.H. Wills Physics Laboratory, University of Bristol, Bristol, United Kingdom*
[49] *Cavendish Laboratory, University of Cambridge, Cambridge, United Kingdom*
[50] *Department of Physics, University of Warwick, Coventry, United Kingdom*
[51] *STFC Rutherford Appleton Laboratory, Didcot, United Kingdom*
[52] *School of Physics and Astronomy, University of Edinburgh, Edinburgh, United Kingdom*
[53] *School of Physics and Astronomy, University of Glasgow, Glasgow, United Kingdom*
[54] *Oliver Lodge Laboratory, University of Liverpool, Liverpool, United Kingdom*
[55] *Imperial College London, London, United Kingdom*
[56] *School of Physics and Astronomy, University of Manchester, Manchester, United Kingdom*
[57] *Department of Physics, University of Oxford, Oxford, United Kingdom*
[58] *Massachusetts Institute of Technology, Cambridge, MA, United States*
[59] *University of Cincinnati, Cincinnati, OH, United States*
[60] *University of Maryland, College Park, MD, United States*
[61] *Syracuse University, Syracuse, NY, United States*

JHEP06(2018)084

[62] *Pontifícia Universidade Católica do Rio de Janeiro (PUC-Rio), Rio de Janeiro, Brazil, associated to*[2]
[63] *University of Chinese Academy of Sciences, Beijing, China, associated to*[3]
[64] *School of Physics and Technology, Wuhan University, Wuhan, China, associated to*[3]
[65] *Institute of Particle Physics, Central China Normal University, Wuhan, Hubei, China, associated to*[3]
[66] *Departamento de Fisica , Universidad Nacional de Colombia, Bogota, Colombia, associated to*[8]
[67] *Institut für Physik, Universität Rostock, Rostock, Germany, associated to*[12]
[68] *National Research Centre Kurchatov Institute, Moscow, Russia, associated to*[32]
[69] *National University of Science and Technology "MISIS", Moscow, Russia, associated to*[32]
[70] *National Research Tomsk Polytechnic University, Tomsk, Russia, associated to*[32]
[71] *Instituto de Fisica Corpuscular, Centro Mixto Universidad de Valencia - CSIC, Valencia, Spain, associated to*[38]
[72] *Van Swinderen Institute, University of Groningen, Groningen, The Netherlands, associated to*[43]
[73] *Los Alamos National Laboratory (LANL), Los Alamos, United States, associated to*[61]

[a] *Universidade Federal do Triângulo Mineiro (UFTM), Uberaba-MG, Brazil*
[b] *Laboratoire Leprince-Ringuet, Palaiseau, France*
[c] *P.N. Lebedev Physical Institute, Russian Academy of Science (LPI RAS), Moscow, Russia*
[d] *Università di Bari, Bari, Italy*
[e] *Università di Bologna, Bologna, Italy*
[f] *Università di Cagliari, Cagliari, Italy*
[g] *Università di Ferrara, Ferrara, Italy*
[h] *Università di Genova, Genova, Italy*
[i] *Università di Milano Bicocca, Milano, Italy*
[j] *Università di Roma Tor Vergata, Roma, Italy*
[k] *Università di Roma La Sapienza, Roma, Italy*
[l] *AGH - University of Science and Technology, Faculty of Computer Science, Electronics and Telecommunications, Kraków, Poland*
[m] *LIFAELS, La Salle, Universitat Ramon Llull, Barcelona, Spain*
[n] *Hanoi University of Science, Hanoi, Vietnam*
[o] *Università di Padova, Padova, Italy*
[p] *Università di Pisa, Pisa, Italy*
[q] *Università degli Studi di Milano, Milano, Italy*
[r] *Università di Urbino, Urbino, Italy*
[s] *Università della Basilicata, Potenza, Italy*
[t] *Scuola Normale Superiore, Pisa, Italy*
[u] *Università di Modena e Reggio Emilia, Modena, Italy*
[v] *MSU - Iligan Institute of Technology (MSU-IIT), Iligan, Philippines*
[w] *Novosibirsk State University, Novosibirsk, Russia*
[x] *National Research University Higher School of Economics, Moscow, Russia*
[y] *Escuela Agrícola Panamericana, San Antonio de Oriente, Honduras*
[z] *School of Physics and Information Technology, Shaanxi Normal University (SNNU), Xi'an, China*
[aa] *Physics and Micro Electronic College, Hunan University, Changsha City, China*
[†] *Deceased*

JHEP06(2018)084